JACS
JOURNAL OF THE AMERICAN CHEMICAL SOCIETY

Communication

pubs.acs.org/JACS

A Bismuth-Halide Double Perovskite with Long Carrier Recombination Lifetime for Photovoltaic Applications

Adam H. Slavney,[†] Te Hu,[§] Aaron M. Lindenberg,[§] and Hemamala I. Karunadasa*[,†]

Departments of [†]Chemistry and [§]Materials Science and Engineering, Stanford University, Stanford, California 94305, United States

Supporting Information

ABSTRACT: Despite the remarkable rise in efficiencies of solar cells containing the lead-halide perovskite absorbers $RPbX_3$ (R = organic cation; X = Br^- or I^-), the toxicity of lead remains a concern for the large-scale implementation of this technology. This has spurred the search for lead-free materials with similar optoelectronic properties. Here, we use the double-perovskite structure to incorporate nontoxic Bi^{3+} into the perovskite lattice in $Cs_2AgBiBr_6$ (**1**). The solid shows a long room-temperature fundamental photoluminescence (PL) lifetime of ca. 660 ns, which is very encouraging for photovoltaic applications. Comparison between single-crystal and powder PL decay curves of **1** suggests inherently high defect tolerance. The material has an indirect bandgap of 1.95 eV, suited for a tandem solar cell. Furthermore, **1** is significantly more heat and moisture stable compared to $(MA)PbI_3$. The extremely promising optical and physical properties of **1** shown here motivate further exploration of both inorganic and hybrid halide double perovskites for photovoltaics and other optoelectronics.

The three-dimensional (3D) hybrid perovskite $RPbI_3$ (R = $CH_3NH_3^+$, $(H_2N)_2CH^+$) has shown great promise as a solar-cell absorber with power-conversion efficiencies for single-junction devices increasing from 4%[1] to 20%[2] in just six years. However, the toxicity of lead is a primary concern for the wide-scale use of this technology, particularly in light of the material's water solubility. The analogous tin perovskite $(MA)SnI_3$ (MA = $CH_3NH_3^+$) has been explored as a nontoxic alternative and efficiencies of devices employing these absorbers have reached ca. 6%.[3] However, the high-lying 5s orbitals of the Sn^{2+} centers render the perovskite unstable to oxidation, limiting the material's viability. Recently, several other nontoxic alternatives consisting of zero- and two-dimensional structures have been explored,[4] but a material with similar optoelectronic properties to $(MA)PbI_3$ has not yet been realized. Here we report the synthesis of the 3D double perovskite $Cs_2Ag^{I}Bi^{III}Br_6$ (**1**, Figure 1A). The material has an indirect bandgap of 1.95 eV, which is suited for coupling with a Si absorber in a tandem solar cell. We measure a notably long room-temperature PL lifetime for **1** of ca. 660 ns. This value is much higher than the recombination lifetime for high-quality $(MA)PbBr_3$ films (170 ns)[5] and approaches the unusually long lifetimes seen in optimized $(MA)PbI_3$ films (736 ns to 1 μs).[6] Importantly, PL decay curves of **1** show that the majority of carriers recombine through this long-lived process, with only a 6% loss in moving from single crystals to powders. This suggests that defects/surface sites will not be detrimental to the material's photovoltaic performance. Furthermore, **1** is much more heat and moisture stable compared to $(MA)PbI_3$. Our results indicate that **1** should be considered as a promising absorber for lead-free perovskite solar cells.

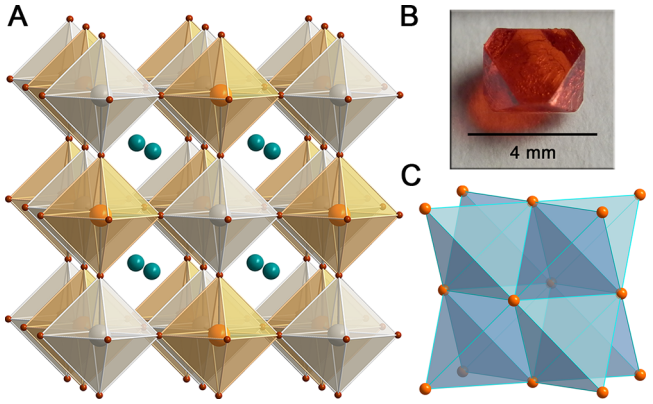

Figure 1. (A) X-ray structure of the ordered double perovskite $Cs_2AgBiBr_6$ (**1**). Orange, gray, turquoise, and brown spheres represent Bi, Ag, Cs, and Br atoms, respectively. (B) Photograph of a single crystal of **1**. (C) The Bi^{3+} face-centered-cubic sublattice in **1**, consisting of edge-sharing tetrahedra.

The bandgap transition of lead-halide perovskites corresponds to a ligand-to-metal charge transfer from the predominantly halide p-orbital-based valence band maximum (VBM) to the conduction band minimum (CBM), which has mostly lead p-orbital character. The $6s^26p^0$ electronic configuration of Pb^{2+} allows for the filled 6s orbital to mix with the iodide 5p orbitals in the valence band, while the vacant lead 6p orbitals form the conduction band.[7] Calculations have identified this VBM and CBM composition as contributing to the material's shallow defect states and long carrier lifetimes, while the high p-orbital-based density of states near the band edges provide for the material's strong absorption.[8] Only three main group elements have stable cations with the $6s^26p^0$ electronic configuration: Tl^+, Pb^{2+}, and Bi^{3+}. Out of these candidates only Bi has low toxicity. In fact Bi has been used for decades as a nontoxic replacement for Pb in areas ranging from organic synthesis to ammunition materials.[9] We therefore focused our efforts on incorporating Bi^{3+} as a B-site cation in the ABX_3 (X = halide) perovskite framework. In 2D halide

Received: December 21, 2015
Published: February 7, 2016

DOI: 10.1021/jacs.5b13294
J. Am. Chem. Soc. 2016, 138, 2138–2141

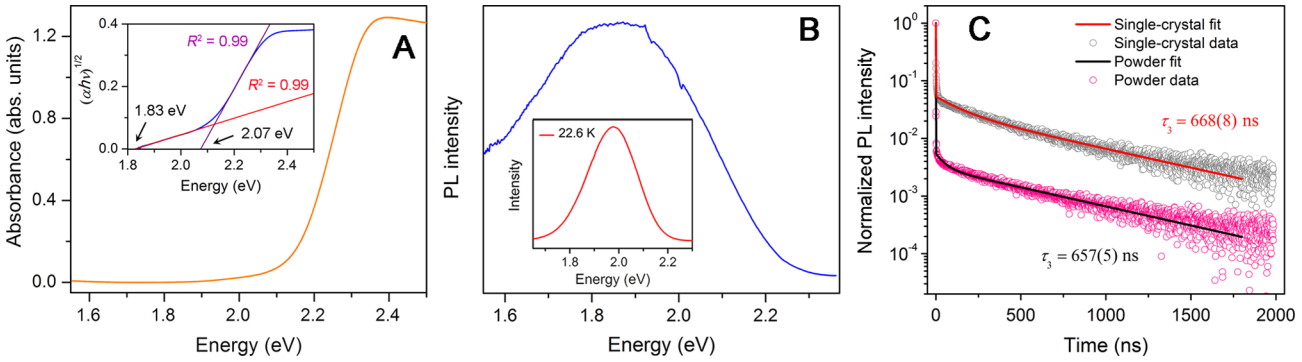

Figure 2. (A) Absorbance spectrum of **1** powder. Inset: Tauc plot showing the characteristics of an indirect band gap. (B) Steady-state room-temperature photoluminescence (PL) spectrum of a powdered sample upon 500 nm excitation. Inset: low-temperature PL spectrum. C) Time-resolved room-temperature PL and fits for the PL decay time (τ) in powder and single-crystal samples.

perovskites, Bi^{3+} has been incorporated into the lattice by introducing vacancies.[10] To accommodate the trivalent Bi^{3+} ion in the 3D perovskite lattice we attempted to incorporate a monovalent metal to yield the double-perovskite structure: $A^{I}_2B^{I}Bi^{III}X_6$.

The oxide double perovskites $A_2BB'O_6$ have been well explored and incorporate a wide variety of metals in various oxidation states.[11] In ordered double perovskites the B and B′ sites alternate in the lattice (Figure 1A). Such perovskites with paramagnetic ions residing only in the B (or B′) sublattice (Figure 1C) have been used for studying exotic magnetic ground states arising from spin frustration.[12] Unusual electronic states such as metallic ferromagnetism[13] and colossal magneto-resistance[14] have also been realized in oxide double perovskites. There are, however, far fewer reports of halide double perovskites. Some examples include the mixed-valence compounds $A_2Au^{I}Au^{III}X_6$ (A = K, Rb, or Cs; X = Cl, Br, or I), which have been explored as potential superconductors,[15] and the cubic perovskites $Cs_2Tl^{I}Tl^{III}X_6$ (X = F or Cl)[16] and $Cs_2AgAuCl_6$.[17] The x = 0.5 member of the solid solution $(MA)Sn_xPb_{1-x}I_3$[18] could also be considered a disordered double perovskite, although the term has not been typically used. Bismuth has been incorporated into the chloride double perovskite $Cs_2NaBiCl_6$, which is a colorless solid.[19]

According to radius-ratio rules that describe packing in ionic solids, Ag^+ is of appropriate size to support octahedral coordination of iodides or bromides in the perovskite lattice. Accordingly, we synthesized the bromide double perovskite: $Cs_2AgBiBr_6$ (**1**). Large single crystals of **1** can be crystallized from a concentrated HBr solution containing stoichiometric CsBr, AgBr, and $BiBr_3$. The perovskite crystallizes as red-orange truncated octahedra in the cubic space group $Fm\bar{3}m$ (Figure 1B). The unit-cell axis of 11.25 Å is roughly double that of $(MA)PbBr_3$ (a = 5.92 Å.)[20] The Ag^+ and Bi^{3+} ions occupy the B and B′ sites in the ordered double-perovskite lattice with slightly different metal-bromide bond lengths. We see no crystallographic evidence for disorder between the Bi and Ag sites.

To evaluate the suitability of **1** for photovoltaic applications we determined its optical bandgap. The perovskite shows the characteristics of an indirect bandgap semiconductor with a shallow absorption region beginning at 1.8 eV followed by a sharp increase in absorption near 2.1 eV (Figure 2A). A Tauc plot of the data, assuming an indirect allowed transition, is shown in the inset of Figure 2A. The linear regions of the plot show the expected phonon-assisted processes, with transitions at 1.83 and 2.07 eV occurring with absorption and emission of a phonon, respectively. This allows us to estimate the indirect bandgap as 1.95 eV with an assisting phonon energy of 0.12 eV. Comparison with the vibrational energies in the Raman spectrum of **1** (Figure S1) indicates that a higher energy phonon mode is involved in the absorption. A Tauc plot, assuming a direct allowed transition, gives a direct bandgap of 2.21 eV (Figure S2), slightly lower than the bandgap of 2.3 eV for $(MA)PbBr_3$.[5] We anticipate that **1** could be used as the higher-bandgap absorber in a tandem solar cell as was recently demonstrated for $(MA)PbI_3$[21] and $(MA)PbBr_3$.[22] Four- and two-terminal tandem cells with Si absorbers require higher-bandgap absorbers with ideal bandgaps of 1.8−2.0 and 1.8−1.9 eV, respectively.[23] Photoelectron spectroscopy in air estimates the VBM for **1** as −6.04 eV with respect to vacuum (Figure S3), similar to that of $(MA)PbBr_3$ (−6.01 eV). Figure 3C shows a comparison of the CBM and VBM of **1** to those of materials relevant to perovskite solar cells.[24]

At room temperature, **1** displays weak PL centered at 1.87 eV (Figure 2B). PL at 23 K is more intense and blueshifted, with the peak centered at 1.98 eV (Figure 2B inset). To determine the fate of photogenerated carriers in **1** we then obtained room-temperature, time-resolved PL data (Figure 2C). The PL intensity shows a fast initial drop followed by a slower decay. Analysis of the entire time trace required three processes: a short-lifetime process (τ_1 < 1 ns), an intermediate-lifetime process (τ_2 = 50−150 ns) and a long-lived component ($\tau_3 \approx$ 660 ns). Time constants for the short and intermediate PL decay processes for single-crystal and powder samples are given in Figures S4 and S5, respectively. While analysis of the short-lived process's lifetime is limited by our instrumental resolution the magnitude of this process (PL intensity × time) is larger in the powder (5%) than in the single crystal (0.02%). Additionally, the lifetime of the intermediate process is much shorter in the powder (54 ns) compared to the single crystal (145 ns). Because powders typically have much more defects and surface states than a single crystal, this suggests that the short- and intermediate-lifetime processes may originate from trap and/or surface-state emission. The long PL decay time of ca. 660 ns does not vary significantly between single-crystal and powder samples and likely gives the material's fundamental recombination lifetime. PL decay curves give the sum of radiative and nonradiative recombination rates. However, the weak PL of **1** indicates that the predominant carrier recombination pathway is nonradiative. Therefore, the PL decay traces in **1** give approximately the nonradiative decay rate

DOI: 10.1021/jacs.5b13294
J. Am. Chem. Soc. 2016, 138, 2138−2141

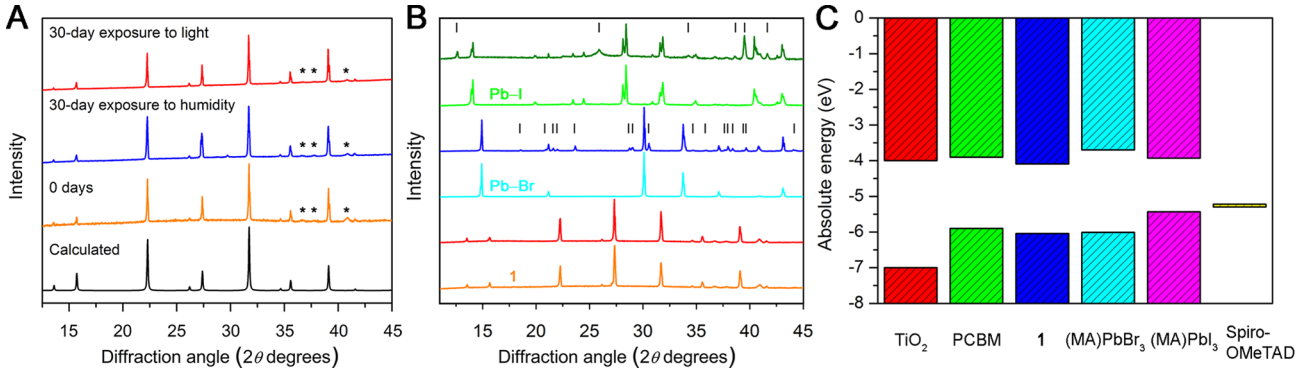

Figure 3. (A) PXRD patterns of **1** after exposure to humidity (55% RH) or light (0.75 Sun). Asterisks denote signals from the sample holder. (B) PXRD patterns of **1** before (orange) and after (red) 72 h at 100 °C, $(MA)PbBr_3$ before (turquoise) and after (blue) 72 h at 60 °C, and $(MA)PbI_3$ before (light green) and after (dark green) 72 h at 60 °C. Vertical bars denote reflections from $PbBr_2$ or PbI_2. (C) CBM and VBM of **1** and other materials[24] relevant to photovoltaic devices with perovskite absorbers.

and the radiative recombination lifetime should be much longer than 660 ns. Long carrier recombination lifetimes are indicators of good photovoltaic performance. These values are significantly higher than those for high-quality $(MA)PbBr_3$ films of 170 ns[5] and approach those for optimized $(MA)PbI_3$ films of 736 ns[6a] to ∼1 μs.[6b] Although indirect bandgap semiconductors typically have longer PL lifetimes compared to direct bandgap materials, the long lifetime in **1** is unusual, especially for powders. Integrating the PL traces, we estimate that 85% of excited carriers emit via a long-lived recombination process ($\tau \geq 660$ ns) in the crystal compared to 80% for the powder (see SI for details). The ratio of these values indicates that faster PL decay components increase by only 6% in powders compared to crystals, attesting to the material's robustness to defects.

As $(MA)PbI_3$ has been shown to be unstable to moisture[25] and noting that silver halides are notoriously light sensitive,[26] we investigated the stability of **1** to both light and moisture. Freshly prepared powders of **1** were stored either in the dark at 55% relative humidity or irradiated at 50 °C with a broad spectrum halogen lamp (0.75 Sun) under dry N_2 for 30 days. PXRD patterns of **1** after moisture or light exposure showed no evidence of material decomposition (Figure 3A). After 15 days some of the irradiated samples showed small localized surface discolorations. These spots recovered their original color upon storing the sample in ambient light for 2 days. Thermal stability is also important for solar-cell absorbers, which can reach temperatures of ca. 50−70 °C during typical device operating conditions[27] and still higher temperatures during device fabrication. Thermogravimetric analysis (TGA) shows that **1** is stable to mass loss up to 430 °C and differential thermal analysis indicates no phase transitions within this temperature range (Figure S6). PXRD patterns obtained after heating **1** at 100 °C in air for 72 h confirms structural integrity (Figure 3B). The absence of volatile organic components likely increases **1**'s thermal stability with respect to $(MA)PbX_3$ (X = I[28] and Br), as shown for $CsPbBr_3$.[29] Although TGA data collected at fast heating rates suggest material stability, $(MA)PbX_3$ slowly loses CH_3NH_2 and HX even at modest temperatures.[28b] PXRD data of $(MA)PbX_3$ heated at 60 °C for 72 h in air show decomposition to PbX_2 (Figure 3B). Although encapsulation may impede this decomposition pathway, inherent thermal stability is an advantage for material processing and its long-term usage.

Our results indicate that **1** preserves many of the desirable properties of $(MA)PbI_3$ and $(MA)PbBr_3$ for solar-cell applications while removing the toxic element, lead. Although Ag can be toxic,[30] the solubility constant for AgBr (K_{sp} at 25 °C = 5×10^{-13}) is ca. 10^4 times lower than for PbI_2, which greatly reduces contamination risks. Substitution of different B-site cations for Ag^I in the double perovskite could further reduce the material's toxicity. Our future efforts will involve device fabrication and evaluation. Standard solution-state film deposition techniques are complicated by the insolubility of AgBr. We are investigating alternative methods for forming the high-quality films required for photovoltaic devices.

Despite the massive interest in perovskite photovoltaics, the $A^IB^{II}X_3$ (X = halide) lattice has proved restrictive for incorporating stable and nontoxic metals. Double perovskites of the form $A_2BB'X_6$ provide a more accommodating platform for substitutions. Here, many combinations of metals in different oxidation states can be incorporated into the B/B′ sublattices, both organic and inorganic cations can be incorporated into the A sites, and the halide can be varied. Our studies show that inorganic and hybrid halide double perovskites should be further investigated for photovoltaic and other optoelectronic applications.

■ ASSOCIATED CONTENT

Supporting Information

The Supporting Information is available free of charge on the ACS Publications website at DOI: 10.1021/jacs.5b13294.

Experimental details, crystallographic data, and spectra, including Figures S1−S9 and Table S1 (PDF)

X-ray crystallographic data for **1** (CIF)

■ AUTHOR INFORMATION

Corresponding Author

*hemamala@stanford.edu

Notes

The authors declare no competing financial interest.

■ ACKNOWLEDGMENTS

This research was funded by the Global Climate and Energy Project (GCEP) and the Alfred P. Sloan Fellowship. Time-resolved PL measurements were funded by the Precourt Institute for Energy. A.H.S. is supported by a Stanford Graduate Fellowship. Single-crystal XRD studies were performed at beamline 11.3.1 at the Advanced Light Source (ALS). The ALS is supported by the Director, Office of

DOI: 10.1021/jacs.5b13294
J. Am. Chem. Soc. 2016, 138, 2138−2141

Science, Office of Basic Energy Sciences, of the U.S. Department of Energy under Contract No. DE-AC02-05CH11231. PXRD studies were done at the Stanford Nanocharacterization Laboratory. We thank Dr. K. Gagnon for help with crystallography, M. A. Manumpil, Dr. Y. Lin, and I. C. Smith for experimental assistance, and Prof. M. D. McGehee for helpful discussions.

REFERENCES

(1) Kojima, A.; Teshima, K.; Shirai, Y.; Miyasaka, T. *J. Am. Chem. Soc.* **2009**, *131*, 6050.
(2) Yang, W. S.; Noh, J. H.; Jeon, N. J.; Kim, Y. C.; Ryu, S.; Seo, J.; Seok, S. I. *Science* **2015**, *348*, 1234.
(3) (a) Noel, N. K.; Stranks, S. D.; Abate, A.; Wehrenfennig, C.; Guarnera, S.; Haghighirad, A. A.; Sadhanala, A.; Eperon, G. E.; Pathak, S. K.; Johnston, M. B.; Petrozza, A.; Herz, L. M.; Snaith, H. J. *Energy Environ. Sci.* **2014**, *7*, 3061. (b) Hao, F.; Stoumpos, C. C.; Cao, D. H.; Chang, R. P. H.; Kanatzidis, M. G. *Nat. Photonics* **2014**, *8*, 489.
(4) (a) Saparov, B.; Hong, F.; Sun, J.-P.; Duan, H.-S.; Meng, W.; Cameron, S.; Hill, I. G.; Yan, Y.; Mitzi, D. B. *Chem. Mater.* **2015**, *27*, 5622. (b) Park, B.-W.; Philippe, B.; Zhang, X.; Rensmo, H.; Boschloo, G.; Johansson, E. M. J. *Adv. Mater.* **2015**, *27*, 6806. (c) Lehner, A. J.; Fabini, D. H.; Evans, H. A.; Hébert, C.-A.; Smock, S. R.; Hu, J.; Wang, H.; Zwanziger, J. W.; Chabinyc, M. L.; Seshadri, R. *Chem. Mater.* **2015**, *27*, 7137. (d) Cortecchia, D.; Dewi, H. A.; Yin, J.; Bruno, A.; Chen, S.; Baikie, T.; Boix, P. P.; Gratzel, M.; Mhaisalkar, S.; Soci, C.; Mathews, N. *Inorg. Chem.* **2016**, *55*, 1044.
(5) Shi, D.; Adinolfi, V.; Comin, R.; Yuan, M.; Alarousu, E.; Buin, A.; Chen, Y.; Hoogland, S.; Rothenberger, A.; Katsiev, K.; Losovyj, Y.; Zhang, X.; Dowben, P. A.; Mohammed, O. F.; Sargent, E. H.; Bakr, O. M. *Science* **2015**, *347*, 519.
(6) (a) Zhou, H.; Chen, Q.; Li, G.; Luo, S.; Song, T.-b.; Duan, H.-S.; Hong, Z.; You, J.; Liu, Y.; Yang, Y. *Science* **2014**, *345*, 542. (b) de Quilettes, D. W.; Vorpahl, S. M.; Stranks, S. D.; Nagaoka, H.; Eperon, G. E.; Ziffer, M. E.; Snaith, H. J.; Ginger, D. S. *Science* **2015**, *348*, 683.
(7) Umebayashi, T.; Asai, K.; Kondo, T.; Nakao, A. *Phys. Rev. B* **2003**, *67*, 155405.
(8) (a) Yin, W.-J.; Yang, J.-H.; Kang, J.; Yan, Y.; Wei, S.-H. *J. Mater. Chem. A* **2015**, *3*, 8926. (b) Du, M. H. *J. Mater. Chem. A* **2014**, *2*, 9091.
(9) Mohan, R. *Nat. Chem.* **2010**, *2*, 336.
(10) Mitzi, D. B. *Inorg. Chem.* **2000**, *39*, 6107.
(11) Vasala, S.; Karppinen, M. *Prog. Solid State Chem.* **2015**, *43*, 1.
(12) (a) Ramirez, A. P. *Annu. Rev. Mater. Sci.* **1994**, *24*, 453. (b) Karunadasa, H. I.; Huang, Q.; Ueland, B. G.; Schiffer, P.; Cava, R. J. *Proc. Natl. Acad. Sci. U. S. A.* **2003**, *100*, 8097.
(13) Erten, O.; Meetei, O. N.; Mukherjee, A.; Randeria, M.; Trivedi, N.; Woodward, P. *Phys. Rev. Lett.* **2011**, *107*, 257201.
(14) Kobayashi, K. I.; Kimura, T.; Sawada, H.; Terakura, K.; Tokura, Y. *Nature* **1998**, *395*, 677.
(15) Kojima, N. *Bull. Chem. Soc. Jpn.* **2000**, *73*, 1445.
(16) Retuerto, M.; Emge, T.; Hadermann, J.; Stephens, P. W.; Li, M. R.; Yin, Z. P.; Croft, M.; Ignatov, A.; Zhang, S. J.; Yuan, Z.; Jin, C.; Simonson, J. W.; Aronson, M. C.; Pan, A.; Basov, D. N.; Kotliar, G.; Greenblatt, M. *Chem. Mater.* **2013**, *25*, 4071.
(17) Elliott, N.; Pauling, L. *J. Am. Chem. Soc.* **1938**, *60*, 1846.
(18) Stoumpos, C. C.; Malliakas, C. D.; Kanatzidis, M. G. *Inorg. Chem.* **2013**, *52*, 9019.
(19) Morss, L. R.; Siegal, M.; Stenger, L.; Edelstein, N. *Inorg. Chem.* **1970**, *9*, 1771.
(20) Weber, D. *Z. Naturforsch., B: Chem. Sci.* **1978**, *33b*, 1443.
(21) Mailoa, J. P.; Bailie, C. D.; Johlin, E. C.; Hoke, E. T.; Akey, A. J.; Nguyen, W. H.; McGehee, M. D.; Buonassisi, T. *Appl. Phys. Lett.* **2015**, *106*, 121105.
(22) Sheng, R.; Ho-Baillie, A. W. Y.; Huang, S.; Keevers, M.; Hao, X.; Jiang, L.; Cheng, Y.-B.; Green, M. A. *J. Phys. Chem. Lett.* **2015**, *6*, 3931.
(23) Beiley, Z. M.; McGehee, M. D. *Energy Environ. Sci.* **2012**, *5*, 9173.
(24) (a) Cho, H.; Jeong, S.-H.; Park, M.-H.; Kim, Y.-H.; Wolf, C.; Lee, C.-L.; Heo, J. H.; Sadhanala, A.; Myoung, N.; Yoo, S.; Im, S. H.; Friend, R. H.; Lee, T.-W. *Science* **2015**, *350*, 1222. (b) Boix, P. P.; Nonomura, K.; Mathews, N.; Mhaisalkar, S. G. *Mater. Today* **2014**, *17*, 16.
(25) (a) Noh, J. H.; Im, S. H.; Heo, J. H.; Mandal, T. N.; Seok, S. I. *Nano Lett.* **2013**, *13*, 1764. (b) Smith, I. C.; Hoke, E. T.; Solis-Ibarra, D.; McGehee, M. D.; Karunadasa, H. I. *Angew. Chem., Int. Ed.* **2014**, *53*, 11232.
(26) Gurney, R. W.; Mott, N. F. *Proc. R. Soc. London, Ser. A* **1938**, *164*, 151.
(27) Strevel, N.; Trippel, L.; Gloeckler, M. *Photovoltaics Int.* **2012**, *17*, 1.
(28) (a) Dualeh, A.; Gao, P.; Seok, S. I.; Nazeeruddin, M. K.; Grätzel, M. *Chem. Mater.* **2014**, *26*, 6160. (b) Conings, B.; Drijkoningen, J.; Gauquelin, N.; Babayigit, A.; D'Haen, J.; D'Olieslaeger, L.; Ethirajan, A.; Verbeeck, J.; Manca, J.; Mosconi, E.; De Angelis, F.; Boyen, H. G. *Adv. Energy Mater.* **2015**, *5*, 1500477.
(29) Kulbak, M.; Gupta, S.; Kedem, N.; Levine, I.; Bendikov, T.; Hodes, G.; Cahen, D. *J. Phys. Chem. Lett.* **2016**, *7*, 167.
(30) Hadrup, N.; Lam, H. R. *Regul. Toxicol. Pharmacol.* **2014**, *68*, 1.

DOI: 10.1021/jacs.5b13294
J. Am. Chem. Soc. 2016, 138, 2138−2141